JOURNAL OF COMPUTATIONAL PHYSICS **146,** 157–180 (1998)
ARTICLE NO. CP985908

Fast Evaluation of Three-Dimensional Transient Wave Fields Using Diagonal Translation Operators

A. Arif Ergin,* Balasubramaniam Shanker,† and Eric Michielssen‡

Center for Computational Electromagnetics, Department of Electrical and Computer Engineering, University of Illinois at Urbana-Champaign, Urbana, Illinois 61801
E-mail: *aergin@decwa.ece.uiuc.edu, †shanker@socrates.ece.uiuc.edu, and ‡michiels@decwa.ece.uiuc.edu

Received October 1, 1997

This paper presents novel plane wave time domain (PWTD) algorithms which accelerate the computational analysis of transient surface scattering phenomena. The proposed PWTD algorithms permit the fast evaluation of transient fields satisfying the wave equation. The cost associated with the computation of fields at N_s observers produced by a surface bound source density represented in terms of N_s spatial samples for N_t time steps scales as $O(N_t N_s^2)$ if classical time domain integral-equation-based methods are used. It is shown that this cost can be reduced to $O(N_t N_s^{4/3} \log N_s)$ and $O(N_t N_s \log N_s)$ using two-level and multilevel PWTD schemes, respectively. These algorithms are the time domain counterparts of frequency domain fast multipole methods and make feasible the practical broadband analysis of scattering from large and complex bodies.

Key Words: integral equations; time domain; plane wave time domain (PWTD); slant stack transform (SST); computational complexity.

1. INTRODUCTION

Recently, the scientific community has expressed a renewed interest in the analysis of short-pulse radiation and transient scattering phenomena [1–8]. The characterization of transient wave phenomena is of paramount importance in disciplines ranging from electromagnetics to acoustics, elastodynamics, and geophysics. Efficient computational analysis of these phenomena hinges upon the availability of fast time domain algorithms.

Today, all prevailing time domain techniques for analyzing wave scattering phenomena are differential-equation based. Examples include the finite difference time domain (FDTD) technique [9] and the time domain finite element method [10]. These techniques rely on a volumetric discretization of the structure under consideration and require local boundary conditions for grid truncation. As such, they are not well suited for analyzing free-space

0021-9991/98 $25.00

surface scattering problems because the number of unknowns scales proportionally to the volume of the computational domain containing the scatterer and inexact local absorbing boundary conditions have to be used to emulate the radiation condition. Furthermore, for large bodies, additional steps have to be taken to overcome grid dispersion errors, adding to the computational cost of these algorithms. For free-space surface radiation and scattering problems, time domain integral-equation (TDIE)-based methods appear to be preferable to differential-equation-based techniques because (i) they only require a discretization of the scatterer surface, (ii) they implicitly impose the radiation condition, and (iii) they are devoid of grid dispersion errors. Unfortunately, TDIE techniques have long been conceived as intrinsically unstable and computationally expensive when compared to their differential-equation counterparts. However, recently, progress toward stable TDIE-based schemes has been reported [11–15]. In contrast, literature on techniques for reducing the computational complexity of these TDIE techniques is virtually nonexistent. This is in spite of the fact that the last decade has witnessed significant speedup of frequency domain integral equation solvers with the advent of the fast multipole method (FMM) [16–19], the impedance matrix localization technique [20], the multilevel matrix decomposition algorithm [21], etc. Although the structure of transient wave fields has been well studied [2, 6, 22–24], to our knowledge no TDIE algorithms with reduced computational complexity have been reported. Recently, preliminary research has indicated that fast methods, similar in spirit to the frequency domain algorithms, can also be developed in the time domain [25]. The purpose of this paper is to introduce novel fast time domain algorithms that are based on plane wave expansions. These algorithms result in a significant reduction of the computational cost associated with the analysis of surface scattering problems when used in tandem with TDIE-based techniques such as the well-known marching-on-in-time (MOT) method [3, 4].

Differential and classical integral-equation-based schemes for analyzing transient wave phenomena suffer from a high computational cost. Consider a surface scatterer of area S which resides in a homogeneous three-dimensional space (Fig. 1) and which is excited by a pulse whose temporal spectrum vanishes for $\omega > \omega_{\max}$. Integral-equation-based approaches model the fields scattered from the surface as those produced by induced surface sources. Since the sum of the incident and scattered fields satisfies certain boundary conditions on

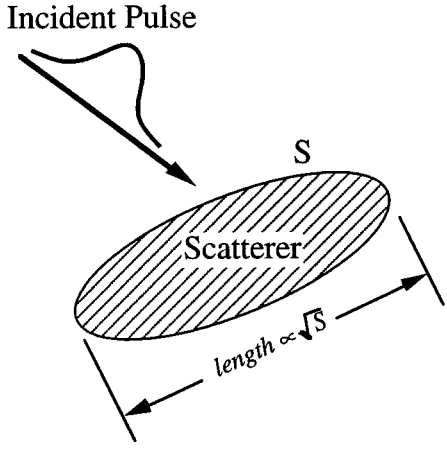

FIG. 1. Scattering problem under consideration.

the surface of the scatterer, an integral equation relating the incident field on the scatterer to the field produced by all current and past sources can be constructed. Assuming that the induced surface sources reside on the scatterer surface for a duration T, after which they become vanishingly small, the source distribution can be discretized and represented in terms of $N_s \propto S(\omega_{\max}/c)^2$ spatial and $N_t \propto T\omega_{\max}$ temporal samples. Here, c denotes the wave speed in the medium. Discretization of the integral equation results in a time marching procedure for computing the induced sources. Updating the source distribution requires the computation of the field at N_s observers due to all N_s sources. Since this computation has to be performed for all time steps, the computational complexity associated with this classical MOT procedure scales as $O(N_t N_s^2)$. Alternatively, if this problem is analyzed using FDTD, $O(N_s^{2.25})$ volumetric field quantities must be updated for all $O(N_t N_s^{0.25})$ time steps, resulting in a computational complexity of $O(N_t N_s^{2.5})$. These estimates reflect the fact that FDTD mesh sizes become smaller as the problem size grows in order to minimize the build up of phase dispersion errors throughout the mesh [26].

This paper introduces diagonalized time domain translation operators which permit the rapid evaluation of transient fields produced by surface-bound source distributions. These diagonalized translation operators can be used in tandem with classical integral-equation-based techniques for analyzing transient scattering phenomena. It will be shown that the computational complexities associated with the solution of large scale surface scattering problems using the proposed two-level and multilevel fast plane wave time domain (PWTD) algorithms scale as $O(N_t N_s^{4/3} \log N_s)$ and $O(N_t N_s \log N_s)$, respectively. Computer codes based on these PWTD algorithms are expected to outperform classical MOT and FDTD codes for sufficiently large surface scatterers.

This paper is organized as follows. Section 2 introduces a diagonalized translation operator for time domain fields that satisfy the scalar wave equation, for both continuous and sampled field representations. Section 3 discusses the practical implementation of the PWTD algorithm, validates the algorithm through numerical examples, and analyzes the computational complexity of this algorithm when used in conjunction with MOT schemes. Finally, Section 4 presents our conclusions.

2. A DIAGONALIZED TIME DOMAIN TRANSLATION OPERATOR

This section introduces plane wave representations for transient fields and derives a diagonalized time domain translation operator together with space-time constraints that ensure its validity and applicability in a time marching algorithm. A closed-form expression for the translation function for sampled field representations is also derived.

2.1. *Preliminaries*

Consider a source distribution $q(\mathbf{r}, t)$ residing in a source sphere of radius R_s centered around $\mathbf{r}^{c(s)}$ and radiating in an unbounded, nondispersive, and homogeneous medium (Fig. 2a). The field $u(\mathbf{r}, t)$ produced by $q(\mathbf{r}, t)$ is to be evaluated at observers distributed throughout an observation sphere of radius R_o centered around $\mathbf{r}^{c(o)}$. Let $\mathbf{R}_c = \mathbf{r}^{c(o)} - \mathbf{r}^{c(s)}$ denote the vector connecting the source and observation sphere centers. Without loss of generality, it is assumed that $R_o = R_s$ and that $\mathbf{R}_c = R_c\hat{\mathbf{z}}$, where $R_c = |\mathbf{R}_c|$.

The field $u(\mathbf{r}, t)$ satisfies the wave equation

$$\nabla^2 u(\mathbf{r}, t) - \frac{1}{c^2}\frac{\partial^2}{\partial t^2} u(\mathbf{r}, t) = -q(\mathbf{r}, t). \tag{1}$$

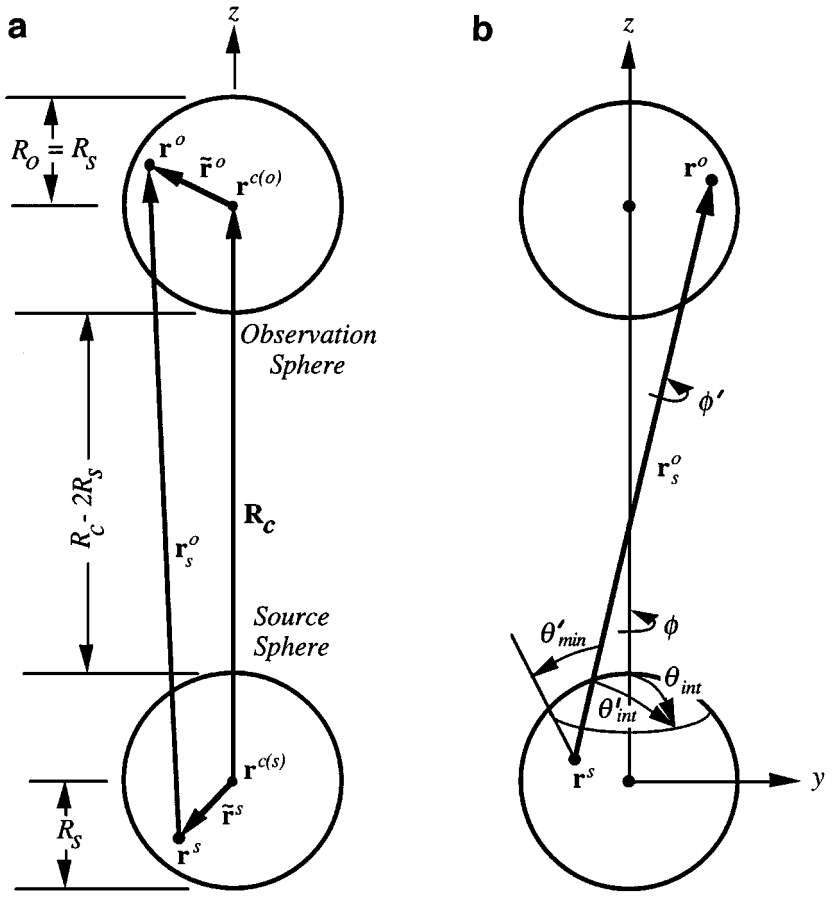

FIG. 2. (a) The geometry of the problem. (b) Definition of angles in primed coordinate system. (c) Relevant dimensions for ray translation.

The field at an observer located at $\mathbf{r}^o$ can be succinctly expressed as

$$u(\mathbf{r}^o, t) = \int_{V_s} d\mathbf{r}' \frac{q(\mathbf{r}', t - |\mathbf{r}^o - \mathbf{r}'|/c)}{4\pi|\mathbf{r}^o - \mathbf{r}'|}, \tag{2}$$

where V_s denotes the volume of the source sphere. If $q(\mathbf{r}, t)$ consists of a point source located at $\mathbf{r}^s$ with a time signature $f(t)$, i.e., if

$$q(\mathbf{r}, t) = f(t)\delta(\mathbf{r} - \mathbf{r}^s), \tag{3}$$

where $\delta(\cdot)$ is a Dirac impulse, then the field observed at $\mathbf{r}^o$ is

$$u(\mathbf{r}^o, t) = \frac{f\left(t - r_s^o/c\right)}{4\pi r_s^o}, \tag{4}$$

where $r_s^o = |\mathbf{r}_s^o|$ and $\mathbf{r}_s^o = \mathbf{r}^o - \mathbf{r}^s$. Henceforth, to simplify the notation, the positions of the

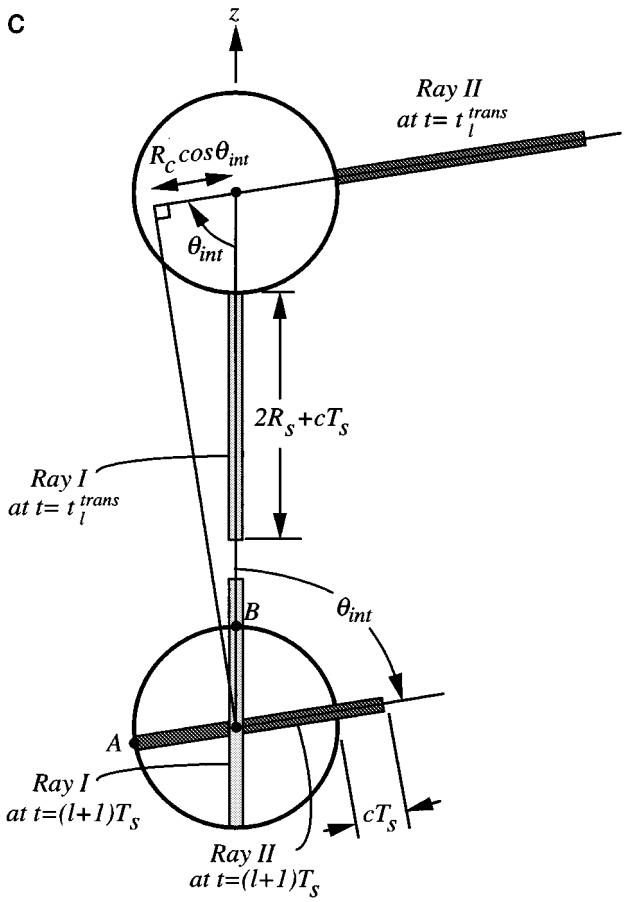

FIG. 2—*Continued*

source and observation points relative to their respective sphere centers are denoted by $\tilde{\mathbf{r}}^s = \mathbf{r}^s - \mathbf{r}^{c(s)}$ and $\tilde{\mathbf{r}}^o = \mathbf{r}^o - \mathbf{r}^{c(o)}$.

If multiple sources are present, the observer field is evaluated by aggregating partial fields (4) due to all sources. This process is repeated for multiple observers if necessary. The computational cost of this operation is proportional to the number of sources and observers, as well as the required number of temporal field samples and hence scales unfavorably. It is well known that the cost of the frequency domain counterpart of this operation can be considerably reduced by using the FMM. Instead of directly evaluating the field at each observer due to all sources, the FMM relies on a three-stage process of aggregation, translation, and disaggregation to efficiently compute observer fields. The associated reduction in computational complexity is due to the fact that the frequency domain translation operator is diagonal when expressed in a plane wave basis [17, 27].

2.2. *A Plane Wave Representation*

As a first step toward representing the field $u(\mathbf{r}^o, t)$ as a superposition of plane waves, the source signal $f(t)$ of duration T is artificially broken up into L subsignals $f_l(t)$,

$l = 0, \ldots, L-1$ of duration $T_s = T/L$ such that

$$f(t) = \sum_{l=0}^{L-1} f_l(t), \tag{5}$$

where $f_l(t) = 0$ for $t < lT_s$ and $t \geq (l+1)T_s$. Let $q_l(\mathbf{r}, t)$ denote the source distribution associated with the subsignal active during time interval l, i.e.,

$$q_l(\mathbf{r}, t) = f_l(t)\delta(\mathbf{r} - \mathbf{r}^s), \tag{6}$$

and let $u_l(\mathbf{r}^o, t)$ denote the field at $\mathbf{r}^o$ due to $q_l(\mathbf{r}, t)$. Then,

$$q(\mathbf{r}, t) = \sum_{l=0}^{L-1} q_l(\mathbf{r}, t) \tag{7}$$

and

$$u(\mathbf{r}^o, t) = \sum_{l=0}^{L-1} u_l(\mathbf{r}^o, t). \tag{8}$$

To arrive at a plane wave representation of $u_l(\mathbf{r}^o, t)$, consider the field $\tilde{u}_l(\mathbf{r}^o, t)$ defined by

$$\tilde{u}_l(\mathbf{r}^o, t) = -\frac{1}{8\pi^2 c}\frac{\partial}{\partial t}\int_0^{2\pi} d\phi \int_0^{\theta_{\text{int}}} d\theta \sin\theta \tilde{q}_l\big(\hat{\mathbf{k}}, t - \hat{\mathbf{k}} \cdot \mathbf{r}^o_{c(s)}/c\big). \tag{9}$$

where $\mathbf{r}^o_{c(s)} = \mathbf{r}^o - \mathbf{r}^{c(s)}$, $\hat{\mathbf{k}} = \hat{\mathbf{x}}\sin\theta\cos\phi + \hat{\mathbf{y}}\sin\theta\sin\phi + \hat{\mathbf{z}}\cos\theta$, and $\tilde{q}_l(\hat{\mathbf{k}}, t)$ is the slant stack transform (SST) of the source distribution $q_l(\mathbf{r}, t)$ [8, 28] defined by

$$\tilde{q}_l(\hat{\mathbf{k}}, t) = \int_{V_s} d\mathbf{r}' q_l\big(\mathbf{r}', t + \hat{\mathbf{k}} \cdot \big(\mathbf{r}' - \mathbf{r}^{c(s)}\big)/c\big). \tag{10}$$

Note that, in Eq. (9), the integration is over a cap of the unit sphere for which $\theta \leq \theta_{\text{int}}$. For the source configuration specified in Eq. (6), the SST is given by

$$\tilde{q}_l(\hat{\mathbf{k}}, t) = f_l(t + \hat{\mathbf{k}} \cdot \tilde{\mathbf{r}}^s/c). \tag{11}$$

To gain insight into the relationship between $\tilde{u}_l(\mathbf{r}^o, t)$ and $u_l(\mathbf{r}^o, t)$, (11) is substituted into Eq. (9) to obtain

$$\tilde{u}_l(\mathbf{r}^o, t) = -\frac{1}{8\pi^2 c}\frac{\partial}{\partial t}\int_0^{2\pi} d\phi \int_0^{\theta_{\text{int}}} d\theta \sin\theta f_l\big(t - \hat{\mathbf{k}} \cdot \mathbf{r}^o_s/c\big). \tag{12}$$

Next, the above integral is evaluated by transforming the integration variables (θ, ϕ) to a new set of angular coordinates (θ', ϕ') which are defined with respect to the axis aligned with the vector $\mathbf{r}^o_s$ as shown in Fig. 2b. In this new coordinate system, the upper limit on θ', θ'_{int}, depends on ϕ', $\mathbf{r}^o$, and $\mathbf{r}^s$, and

$$\tilde{u}_l(\mathbf{r}^o, t) = -\frac{1}{8\pi^2 c}\frac{\partial}{\partial t}\int_0^{2\pi} d\phi' \int_0^{\theta'_{\text{int}}(\phi', \mathbf{r}^o, \mathbf{r}^s)} d\theta' \sin\theta' f_l\big(t - \hat{\mathbf{k}}' \cdot \mathbf{r}'^o_s/c\big), \tag{13}$$

where $\hat{\mathbf{k}}' = \hat{\mathbf{x}}' \sin\theta' \cos\phi' + \hat{\mathbf{y}}' \sin\theta' \sin\phi' + \hat{\mathbf{z}}' \cos\theta'$, and $\mathbf{r}_s'^o = \hat{\mathbf{z}}' r_s^o$. In deriving the limits on the elevation integral in (13), it was tacitly assumed that

$$\theta_{\text{int}} > \cos^{-1}\left(\frac{\hat{\mathbf{z}} \cdot \mathbf{r}_s^o}{r_s^o}\right). \tag{14}$$

Using $\hat{\mathbf{k}}' \cdot \mathbf{r}_s'^o = r_s^o \cos\theta'$ and setting $\tau = (r_s^o/c)\cos\theta'$ in (13) yields

$$\begin{aligned}
\tilde{u}_l(\mathbf{r}^o, t) &= -\frac{1}{8\pi^2 r_s^o} \frac{\partial}{\partial t} \int_0^{2\pi} d\phi' \int_{(r_s^o/c)\cos\theta'_{\text{int}}(\phi', \mathbf{r}^o, \mathbf{r}^s)}^{r_s^o/c} d\tau \; f_l(t-\tau) \\
&= \frac{1}{8\pi^2 r_s^o} \int_0^{2\pi} d\phi' \left[f_l\left(t - \frac{r_s^o}{c}\right) - f_l\left(t - \frac{r_s^o}{c}\cos\theta'_{\text{int}}(\phi', \mathbf{r}^o, \mathbf{r}^s)\right)\right] \\
&= \frac{1}{4\pi r_s^o} f_l\left(t - \frac{r_s^o}{c}\right) - \frac{1}{8\pi^2 r_s^o} \int_0^{2\pi} d\phi' \, f_l\left(t - \frac{r_s^o}{c}\cos\theta'_{\text{int}}(\phi', \mathbf{r}^o, \mathbf{r}^s)\right).
\end{aligned} \tag{15}$$

In the last expression, the first term corresponds to the true observer field $u_l(\mathbf{r}^o, t)$. Note that, were it not for the second term, which will be referred to as the ghost signal, $\tilde{u}_l(\mathbf{r}^o, t)$ would be identical to $u_l(\mathbf{r}^o, t)$. The above derivation closely follows that of Heyman [6], who generalizes the results of Tygel and Hubral [2]. Equations (12) and (15) imply that, if the ghost signal can somehow be removed from $\tilde{u}_l(\mathbf{r}^o, t)$, the true observer field can be constructed as a superposition of plane waves using techniques that are akin to those underlying the frequency-domain fast multipole method. In what follows, a scheme is derived that permits one to time gate $\tilde{u}_l(\mathbf{r}^o, t)$ in order to retain only the true observer field.

It can be verified that (14) holds for arbitrary source and observer locations $\mathbf{r}^s$ and $\mathbf{r}^o$ chosen within the source and observation spheres provided that

$$\theta_{\text{int}} > \sin^{-1}(2R_s/R_c). \tag{16}$$

From Eq. (15) it follows that the ghost signal present in $\tilde{u}_l(\mathbf{r}^o, t)$ vanishes after

$$\begin{aligned}
t_l^{\text{ghost}} &= \frac{r_s^o}{c}\cos\theta'_{\min} + (l+1)T_s \\
&< (R_c \cos\theta_{\text{int}} + 2R_s)/c + (l+1)T_s,
\end{aligned} \tag{17}$$

where $\theta'_{\min} = \min[\theta'_{\text{int}}(\phi', \mathbf{r}^o, \mathbf{r}^s)]$, and the upper bound follows from geometrical considerations (see Fig. 2c). The fields in the observation sphere coincide with the true fields after the ghost signal has vanished. Also, the true field does not reach the observation sphere before

$$t_l^{\text{trans}} = (R_c - 2R_s)/c + lT_s. \tag{18}$$

Therefore, provided that $t_l^{\text{trans}} > t_l^{\text{ghost}}$, all ghost fields in the observation sphere cease to exist before the true signal arrives. In addition, if $t_l^{\text{trans}} > (l+1)T_s$, all source activity related to the lth time interval ends before the true signal reaches any observer. In summary,

$$t_l^{\text{trans}} \geq t_l^{\text{ghost}} \Rightarrow u_l(r^o, t) = \begin{cases} 0 & t < t_l^{\text{trans}} \\ \tilde{u}_l(r^o, t) & t \geq t_l^{\text{trans}} \end{cases}, \tag{19}$$

$$t_l^{\text{trans}} \geq (l+1)T_s \Rightarrow f_l(t) = 0, \quad t \geq t_l^{\text{trans}}. \tag{20}$$

The above two conditions can be restated, using (17) and (18), as

$$\frac{cT_s}{R_s} \leq \frac{R_c}{R_s} - 2 \tag{21}$$

and

$$\frac{cT_s}{R_s} \leq \frac{R_c}{R_s}(1 - \cos\theta_{\text{int}}) - 4. \tag{22}$$

It can be shown that constraint (16) is automatically satisfied provided that (22) holds for any $T_s \geq 0$.

The above two constraints are key to the development of the PWTD algorithm. Equation (19) implies that if, for a given source and observation sphere pair (i.e., for a given R_c/R_s), a cT_s/R_s and a θ_{int} that satisfy both (21) and (22) are selected, then the field $u(\mathbf{r}^o, t)$ can be reconstructed as a superposition of time-gated $\tilde{u}_l(\mathbf{r}^o, t)$. The contribution of each of the time-gated $\tilde{u}_l(\mathbf{r}^o, t)$ to the observed field can be obtained by translating the SST of the source distribution $q_l(\mathbf{r}, t)$ at $t = t_l^{\text{trans}}$. It is easily recognized that the SST of $q_l(\mathbf{r}, t)$ corresponds to "outgoing" rays, leaving the source sphere; similarly, it will be shown in the next subsection that after translation (i.e., after $t = t_l^{\text{trans}}$), $u_l(\mathbf{r}^o, t)$ can be described in terms of "incoming" rays impinging upon the observation sphere. Condition (21) ensures that this SST can be completely constructed prior to the translation time, enabling the PWTD algorithm to be incorporated into any time marching scheme.

In practice, provided that a cT_s/R_s that satisfies (21) is chosen for a given R_c/R_s, θ_{int} is computed from (22) by enforcing the equality. This procedure minimizes θ_{int} and hence will minimize the computational cost associated with the numerical procedure for evaluating $\tilde{u}_l(\mathbf{r}^o, t)$, as described in Section 3. For this choice of cT_s/R_s and θ_{int}, it follows from (17)–(19) that at $t = t_l^{\text{trans}}$, the ray traveling along $\theta = 0$ is about to enter the observation sphere, while rays traveling along directions $\theta = \theta_{\text{int}}$ have all exited the sphere (Fig. 2c). At $t = t_l^{\text{trans}}$, rays traveling at intermediate angles partially overlap with the observation sphere, but add up to a null field in its interior.

The implications of inequalities (21) and (22) are further illustrated in Fig. 3. For a given R_c/R_s, combinations of θ_{int} and cT_s/R_s that satisfy both (21) and (22) lie to the lower right of the intersection of the curves obtained by enforcing the equalities in (21) and (22). For example, while the point $(\theta_{\text{int}}, cT_s/R_s) = (120^\circ, 15)$ permits a ghost-free solution for $R_c/R_s = 20$, this same combination does not permit a ghost-free solution for $R_c/R_s = 10$. Note that as the two spheres approach each other, the region that satisfies both conditions collapses to the point $(\theta_{\text{int}}, cT_s/R_s) = (180^\circ, 0)$.

2.3. *Closed-Form Translation Function for Sampled Field Representations*

Equation (9), together with constraints (21) and (22), is the basis for formulating the PWTD algorithm for sampled field representations. In practice, $u(\mathbf{r}^o, t)$ is evaluated by assuming that the source distribution $q(\mathbf{r}, t)$ is temporally bandlimited, i.e., the temporal spectrum of $f(t)$ vanishes for $\omega > \omega_{\max}$. Hence, $f(t)$ can be sampled and locally interpolated using temporally bandlimited and approximately timelimited functions as

$$f(t) \cong \sum_{k=1}^{N_t} f(k\Delta t) P_k(t), \tag{23}$$

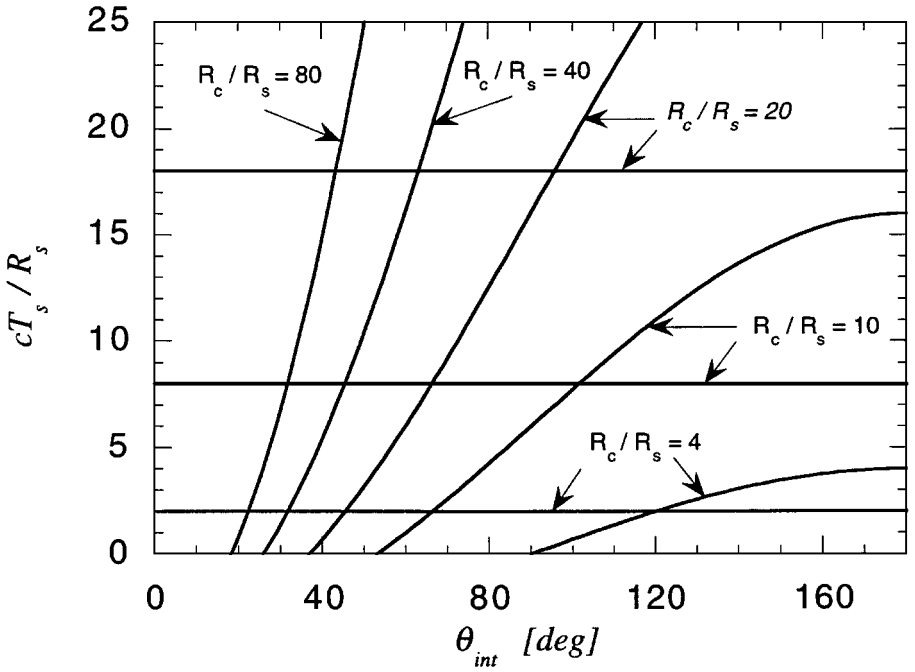

FIG. 3. Graphical representation of the constraints (21) and (22) for different values of R_c/R_s.

where Δt is the time step size and $P_k(t)$ is a bandlimited interpolant [29]. Many choices for the interpolation function exist, however, a near optimal one—a variant of the approximate prolate spheroidal (APS) functions introduced by Knab [30]—is given by

$$P_k(t) = \frac{\omega_o}{\omega_s} \frac{\sin(\omega_o(t-k\Delta t))}{\omega_o(t-k\Delta t)} \frac{\sinh\left(\frac{\pi}{2} p_t(1-1/\chi_o)\sqrt{1-[(t-k\Delta t)/p_t\Delta t]^2}\right)}{\sinh\left(\frac{\pi}{2} p_t(1-1/\chi_o)\right)\sqrt{1-[(t-k\Delta t)/p_t\Delta t]^2}}, \quad (24)$$

where

$$\omega_s = \pi/\Delta t = \chi_o \omega_{\max}, \quad (25)$$

$$\omega_o = (\omega_s + \omega_{\max})/2. \quad (26)$$

In the above $\chi_o > 1$ is the oversampling ratio, and p_t is an integer that defines the approximate duration of the interpolation function. In practice, a truncated version of $P_k(t)$, obtained by setting $P_k(t) = 0$ for $|t - k\Delta t| > p_t \Delta t$, is used. The relative interpolation error ε_t introduced by this truncation can be shown to be bounded as [30]

$$|\varepsilon_t| \le \frac{1}{\sinh\left(\frac{\pi}{2} p_t(1-1/\chi_o)\right)}, \quad (27)$$

which decreases exponentially fast with increasing p_t. Hence, Eq. (23) permits local interpolation in terms of $2p_t$ samples.

From Eq. (23), it follows that the source signal $f(t)$ can be broken up into subsignals $f_l(t)$, as in Eq. (5), given by

$$f_l(t) \cong \sum_{k=lM_t}^{(l+1)M_t-1} f(k\Delta t) P_k(t). \tag{28}$$

Each subsignal $f_l(t)$ is defined in terms of M_t samples of the signal $f(t)$ but spans $M_t' = M_t + 2p_t$ time steps. In other words, whereas each subsignal $f_l(t)$ is formed from samples of $f(t)$ in an interval of length $T_s = M_t \Delta t$, the duration of each $f_l(t)$ is $T_s' = M_t' \Delta t$, and adjacent subsignals overlap by $2p_t$ samples. Obviously, the total number of time samples equals $N_t = LM_t$. Since the interpolation function $P_k(t)$ is bandlimited to ω_s, so is each subsignal $f_l(t)$.

Proceeding with the derivation of a closed-form translation operator, note that

$$\tilde{q}_l\left(\hat{\mathbf{k}}, t - \hat{\mathbf{k}} \cdot \mathbf{r}^o_{c(s)}/c\right) = \delta(t - \hat{\mathbf{k}} \cdot \tilde{\mathbf{r}}^o/c) * \delta(t - \hat{\mathbf{k}} \cdot \mathbf{R}_c/c) * \tilde{q}_l(\hat{\mathbf{k}}, t), \tag{29}$$

where $*$ denotes temporal convolution. Using (29) and (11) in (9) yields

$$\begin{aligned} \tilde{u}_l(\mathbf{r}^o, t) = -\frac{1}{8\pi^2 c} \frac{\partial}{\partial t} \int_0^{2\pi} d\phi \int_0^{\theta_{\text{int}}} d\theta \sin\theta \delta(t - \hat{\mathbf{k}} \cdot \tilde{\mathbf{r}}^o/c) * \delta(t - \hat{\mathbf{k}} \cdot \mathbf{R}_c/c) \\ * \delta(t + \hat{\mathbf{k}} \cdot \tilde{\mathbf{r}}^s/c) * f_l(t). \end{aligned} \tag{30}$$

As mentioned earlier, the SST of the source distribution represented by the last convolution in Eq. (30) can be interpreted as outgoing rays leaving the source sphere. It is seen that for a point source, the SST imposes a direction-dependent shift on $f_l(t)$ by an amount of $\hat{\mathbf{k}} \cdot \tilde{\mathbf{r}}^s/c$ which can be incorporated into Eq. (28). Note that the first convolution in Eq. (30) is the same as the SST except that the direction dependency is reversed. Therefore, $\tilde{u}_l(\mathbf{r}^o, t)$ can be interpreted as a superposition of incoming rays projected onto the observers. However, the use of the interpolation function defined in Eq. (24) implies that knowledge of the field at the edge of the observation sphere requires knowledge of samples from incoming rays that reside p_t samples exterior to the sphere in all directions. Therefore, when working with sampled field representations, constraints (21) and (22) should be satisfied in terms of T_s' and $R_s' = R_s + p_t c \Delta t$, instead of T_s and R_s. Translation times should also be computed in terms of the primed quantities.

To efficiently evaluate $\tilde{u}_l(\mathbf{r}^o, t)$, define

$$\begin{aligned} g_l(\hat{\mathbf{k}}, t) &= \delta(t - \hat{\mathbf{k}} \cdot \tilde{\mathbf{r}}^o/c) * \delta(t + \hat{\mathbf{k}} \cdot \tilde{\mathbf{r}}^s/c) * f_l(t) \\ &= f_l(t - \hat{\mathbf{k}} \cdot (\tilde{\mathbf{r}}^o - \tilde{\mathbf{r}}^s)/c). \end{aligned} \tag{31}$$

The function $g_l(\hat{\mathbf{k}}, t)$ can be interpreted as the time-dependent radiation pattern of a source distribution residing in a sphere of radius $2R_s'$. Therefore, $g_l(\hat{\mathbf{k}}, t)$ is spatially quasi-bandlimited and can be reconstructed to arbitrary precision, provided it is sampled densely enough over the sphere, using the expansion [31]

$$g_l(\hat{\mathbf{k}}, t) = \sum_{n=0}^{M'} \sum_{m=-M_n}^{M_n} g_l(\hat{\mathbf{k}}_{nm}, t) \Omega_{nm}(\hat{\mathbf{k}}), \tag{32}$$

where the functions $\Omega_{nm}(\hat{\mathbf{k}})$ represent bandlimited spherical interpolation functions. As with the temporal interpolants, many different choices for the $\Omega_{nm}(\hat{\mathbf{k}})$ exist. One near optimal choice is a combination of the Dirichlet kernel and the cylindrical APS function introduced by Bucci [31], for which

$$\hat{\mathbf{k}}_{nm} = \hat{\mathbf{x}}\sin\theta_n\cos\phi_{nm} + \hat{\mathbf{y}}\sin\theta_n\sin\phi_{nm} + \hat{\mathbf{z}}\cos\theta_n, \tag{33}$$

$$\phi_{nm} = m2\pi/(2M_n+1), \tag{34}$$

$$\theta_n = n2\pi/(2M'+1), \tag{35}$$

$$M' = \mathrm{Int}(\chi_2 M), \tag{36}$$

$$M = \mathrm{Int}(2\chi_1\omega_s R_s'/c) + 1, \tag{37}$$

$$M_n = \mathrm{Int}\big(2\big[\sin\theta_n + (\chi_1-1)\sin^{1/3}\theta_n\big]\omega_s R_s'/c\big) + 1, \tag{38}$$

$$\Omega_{nm}(\hat{\mathbf{k}}) = \begin{cases} S_0(\theta) & n=0 \\ S_n(\theta)D_{M_n}(\phi-\phi_{nm}) + S_n(-\theta)D_{M_n}(\phi+\pi-\phi_{nm}) & n\neq 0 \end{cases} \tag{39}$$

$$D_{M_n}(\phi) = \frac{\sin[(2M_n+1)\phi/2]}{(2M_n+1)\sin(\phi/2)} \tag{40}$$

$$S_n(\theta) = \frac{R_N(\theta-\theta_n,\, p_s\Delta\theta)}{R_N(0,\, p_s\Delta\theta)} D_{M'}(\theta-\theta_n) \tag{41}$$

$$\Delta\theta = 2\pi/(2M'+1) \tag{42}$$

$$R_N(\theta,\, p_s\Delta\theta) = \frac{\sinh\big[(2N+1)\sinh^{-1}\sqrt{\sin^2(p_s\Delta\theta/2) - \sin^2(\theta/2)}\big]}{\sqrt{\sin^2(p_s\Delta\theta/2) - \sin^2(\theta/2)}}. \tag{43}$$

In the above, $\chi_1 > 1$ is the excess bandwidth factor, $\chi_2 > 1$ is the oversampling ratio in elevation, p_s is an integer that defines the approximate angular extent of $S_n(\theta)$, and $N = M' - M$. As with the temporal interpolation functions, $S_n(\theta)$ can also be truncated for $|\theta-\theta_n| > p_s\Delta\theta$, yielding a relative interpolation error ε_s bounded by

$$|\varepsilon_s| \le \frac{1}{\sinh[\pi p_s(1-1/\chi_2)]}. \tag{44}$$

This error also decreases exponentially fast with increasing p_s. Hence, Eq. (32) permits local interpolation in elevation in terms of $2p_s$ samples.

Substituting expansion (32) in (30), rearranging the terms, and interchanging the order of summations and integrations yield

$$\tilde{u}_l(\mathbf{r}^o, t) = \sum_{n=0}^{M'}\sum_{m=-M_n}^{M_n} \delta(t - \hat{\mathbf{k}}_{nm}\cdot\tilde{\mathbf{r}}^o/c) * \mathcal{T}_{nm}(t) * \delta(t + \hat{\mathbf{k}}_{nm}\cdot\tilde{\mathbf{r}}^s/c) * f_l(t), \tag{45}$$

where

$$\mathcal{T}_{nm}(t) = -\frac{1}{8\pi^2 c}\frac{\partial}{\partial t}\int_0^{2\pi} d\phi \int_0^{\theta_{\mathrm{int}}} d\theta\,\sin\theta\,\Omega_{nm}(\hat{\mathbf{k}})\delta(t - \hat{\mathbf{k}}\cdot\mathbf{R}_c/c) \tag{46}$$

is the translation function. Since $\hat{\mathbf{k}}\cdot\mathbf{R}_c = R_c\cos\theta$, the integral in Eq. (46) can be evaluated

in closed form and the translation function can be succinctly expressed as

$$\mathcal{T}_{nm}(t) = -\frac{1}{4\pi R_c(2M_n+1)}\frac{\partial}{\partial t}\Psi_n\left(\cos^{-1}\frac{ct}{R_c}\right) \quad \text{for } \frac{R_c}{c}\cos\theta_{\text{int}} \le t \le \frac{R_c}{c}, \quad (47)$$

where

$$\Psi_n(\theta) = \begin{cases} S_0(\theta) & n = 0 \\ S_n(\theta) + S_n(-\theta) & n \neq 0 \end{cases}. \quad (48)$$

Another useful expression for $\mathcal{T}_{nm}(t)$ results upon expanding the spatially bandlimited and even functions $\Psi_n(\theta)$ in a cosine series as

$$\Psi_n(\theta) = \sum_{k=0}^{M'+N} a_{n,k}\cos(k\theta). \quad (49)$$

Substituting (49) into (47), and using the relation $T_k(x) = \cos(k\cos^{-1}x)$, where $T_k(x)$ is the kth order Chebyshev polynomial, yields

$$\mathcal{T}_{nm}(t) = -\frac{1}{4\pi R_c(2M_n+1)}\frac{\partial}{\partial t}\sum_{k=0}^{M'+N} a_{n,k}T_k\left(\frac{ct}{R_c}\right) \quad \text{for } \frac{R_c}{c}\cos\theta_{\text{int}} \le t \le \frac{R_c}{c}. \quad (50)$$

Equation (50) shows that the translation function can be expressed as a finite-order polynomial. The sum in Eq. (50) can be efficiently evaluated using Clenshaw's recurrence algorithm [32].

To elucidate the properties of the translation function, the functions $\Psi_n(\theta)$ are plotted with respect to θ for $n = 0, \ldots, 10$, $M = 4$, $M' = 10$, and $p_s = 3$ in Fig. 4a. The corresponding time signals $\Psi_n(\cos^{-1}(ct/R_c))$ are shown in Fig. 4b as a function of the time parameter $\tau = ct/R_c$. Clearly, the duration of the translation function is $(1-\cos\theta_{\text{int}})R_c/c$. If θ_{int} is chosen as outlined in the concluding paragraph of Subsection 2.2, i.e., by enforcing the equality in (22) for a T_s'/cR_s' that satisfies constraint (21), this duration equals $T_s' + 4R_s'/c$. However, a truncated version of $\Psi_n(\theta)$ may be used because $S_n(\theta)$ is vanishingly small for $|\theta - \theta_n| > p_s\Delta\theta$. As can be seen in Fig. 4, the translation function associated with the directions for which $\theta_n > \theta_{\text{int}} + p_s\Delta\theta$ vanishes as $\Psi_n(\theta) \cong 0$ for $0 < \theta < \theta_{\text{int}}$. The Ψ_n associated with these directions ($n = 7, \ldots, 10$) are plotted with dash-dotted lines in Fig. 4. For other directions, the nonvanishing portion of Ψ_n in the interval $0 < \theta < \theta_{\text{int}}$ contributes to the translation function and is plotted with a solid line in Fig. 4. Note, however, that for these directions, the duration of the translation function may become much shorter than $T_s' + 4R_s'/c$. Also, if T_s' is fixed, constraint (22) dictates that, as the spheres move further apart, the number of contributing directions decreases.

The above analysis can easily be extended to source and observation spheres for which $\mathbf{R}_c$ is not aligned with the z-axis. One approach is to use interpolation functions that are windowed in both elevation and azimuth instead of the above-introduced interpolants that are windowed solely in elevation. Alternatively, instead of relying on the bandlimited nature of the far-field interpolation functions to bandlimit the translation operator as in the above derivation, the translation operator can be explicitly bandlimited, and the integration over the sphere performed using an exact quadrature formula. This procedure leads to a translation function for which the angular and temporal dependences can be expressed in terms of Legendre polynomials [33]. This derivation is akin to the traditional construction of windowed translation operators for frequency domain fast multipole methods [19, 34, 35].

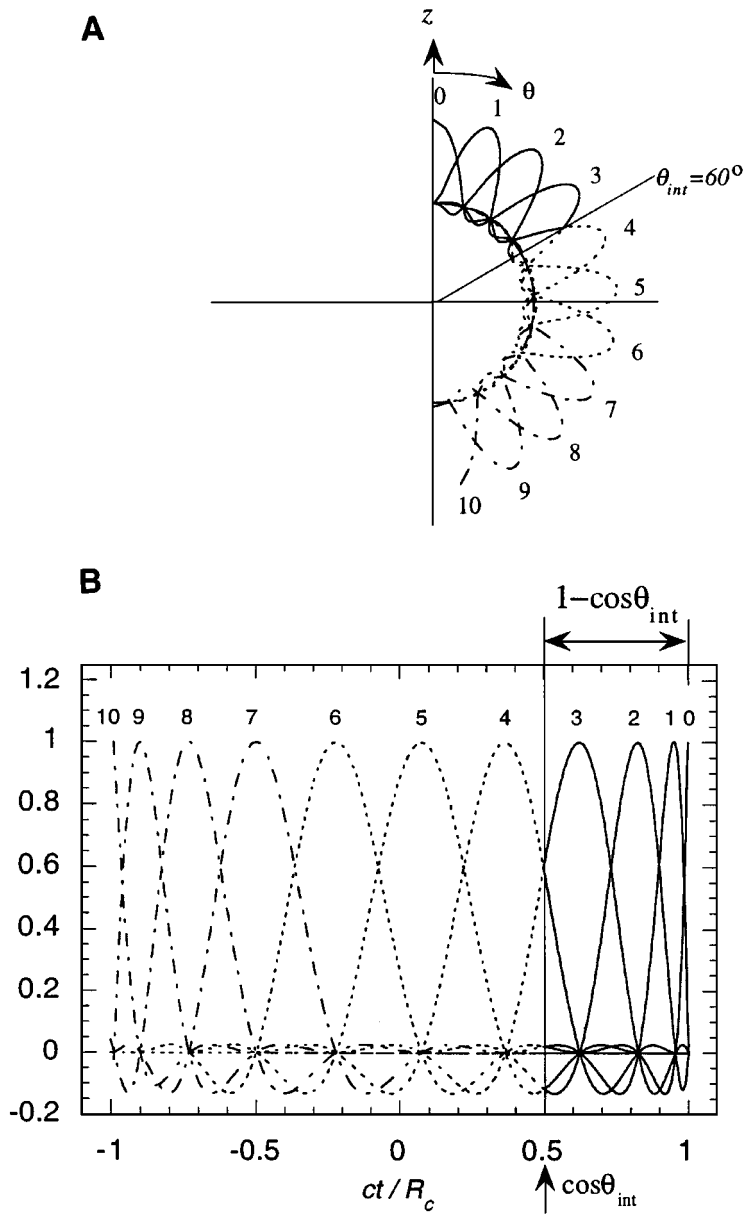

FIG. 4. (a) Interpolation functions $\Psi_n(\theta)$ as a function of θ. (b) Time signals $\Psi_n(\cos^{-1}(ct/R_c))$ as a function of the time parameter $\tau = ct/R_c$.

3. PRACTICAL IMPLEMENTATION AND COMPUTATIONAL COMPLEXITY

This section describes the practical implementation of the PWTD algorithm and studies its computational complexity. Subsection 3.1 outlines the use of the PWTD for evaluating fields at multiple observers due to multiple sources residing in geometrically separate observation and source spheres. This section also describes a series of numerical tests that were conducted to validate the algorithm. Subsections 3.2 and 3.3 comment on the use of the PWTD algorithm for scattering computations in a two-level and a multilevel framework, respectively.

3.1. *Sphere-to-Sphere Translation*

This section outlines a sequence of operations leading to a successful implementation of the PWTD algorithm for computing observer fields. Here, we expand our viewpoint and assume that $q(\mathbf{r}, t)$ consists of M_s point sources located at $\mathbf{r}^{s(j)}$, $j = 1, \ldots, M_s$, distributed throughout the source sphere and characterized by temporal signatures $f^j(t)$, i.e.,

$$q(\mathbf{r}, t) = \sum_{j=1}^{M_s} f^j(t)\delta\left(\mathbf{r} - \mathbf{r}^{s(j)}\right). \tag{51}$$

It is assumed that the spectra of all $f^j(t)$ vanish for $\omega > \omega_{\max}$. The field due to $q(\mathbf{r}, t)$ is to be evaluated at M_o observers located at $\mathbf{r}^{o(i)}$, $i = 1, \ldots, M_o$, distributed throughout the observation sphere. To simplify the notation, the positions of the source and observation points relative to their respective sphere centers are denoted by $\tilde{\mathbf{r}}^{s(j)} = \mathbf{r}^{s(j)} - \mathbf{r}^{c(s)}$ and $\tilde{\mathbf{r}}^{o(i)} = \mathbf{r}^{o(i)} - \mathbf{r}^{c(o)}$.

The field at the ith observer is given by

$$u\left(\mathbf{r}^{o(i)}, t\right) = \sum_{j=1}^{M_s} \frac{f^j\left(t - \left|\mathbf{r}^{o(i)} - \mathbf{r}^{s(j)}\right|/c\right)}{4\pi\left|\mathbf{r}^{o(i)} - \mathbf{r}^{s(j)}\right|}. \tag{52}$$

The evaluation of (52) at all M_o observers for all N_t time steps presents a computationally expensive task as its cost scales as $O(N_t M_s M_o)$, which is of $O(N_t M_s^2)$ if $M_o \propto M_s$. This is due to the fact that in a direct evaluation of Eq. (52) for all observers, one has to aggregate the effects of all sources for all time steps.

Alternatively, the fields at the M_o observers can be evaluated using Eq. (45), which, for the source density expressed by (51), takes the form

$$\tilde{u}_l\left(\mathbf{r}^{o(i)}, t\right) = \sum_{n=0}^{M'} \sum_{m=-M_n}^{M_n} \delta\left(t - \hat{\mathbf{k}}_{nm} \cdot \tilde{\mathbf{r}}^{o(i)}/c\right) * \mathcal{T}_{nm}(t) * \sum_{j=1}^{M_s} \delta\left(t + \hat{\mathbf{k}}_{nm} \cdot \tilde{\mathbf{r}}^{s(j)}/c\right) * f_l^j(t), \tag{53}$$

where it is assumed that each source signal $f^j(t)$ is broken up into L subsignals $f_l^j(t)$, $j = 1, \ldots, M_s$. Equation (53) is the crux of the PWTD algorithm and indicates that the fields within the observation sphere can be constructed via a three-step process consisting of source aggregation, ray translation, and ray disaggregation. The aggregation step, which is represented by the innermost summation in Eq. (53), maps the source subsignals onto a set of time-dependent plane waves—henceforth termed *subrays*—propagating along the $\hat{\mathbf{k}}_{nm}$ vectors. The translation step is carried out by convolving these subrays with the translation functions given in Eq. (46). The disaggregation process can be viewed as the reverse of the aggregation process and maps a set of incoming rays onto observer locations.

To implement this algorithm for a given R_s' and R_c, a T_s' is selected (i) which satisfies constraint (21) and (ii) for which $R_s'/(cT_s')$ is of $O(1)$. If it is impossible to satisfy both of these conditions, the fields in the observer sphere should be computed using classical procedures, as the PWTD becomes less efficient. Next, a θ_{int} is computed by enforcing the equality in constraint (22). The following three operations are then performed, for all L time intervals:

(i) Compute the sampled SST of the source distribution for all ray directions (i.e., perform the right most convolution and carry out the innermost summation in Eq. (53)).

(ii) At $t = t_l^{\text{trans}}$, convolve each subray with the translation function on a direction-by-direction basis, and add the resulting subrays onto incoming rays which propagate through the observation sphere (i.e., perform the middle convolution in Eq. (53)).

While in certain cases it is advantageous to perform this convolution directly in the time domain, it is assumed here that the convolution is performed using an FFT. However, care should be exercised, as the translation function is not bandlimited and cannot be sampled without aliasing. On the other hand, since each subray is bandlimited, so is the result of the convolution. In practice, the Fourier transform of the translation function is evaluated analytically at the frequency points required by the FFT. This is efficiently accomplished by locally expanding the translation function in terms of a small set of orthogonal polynomials whose Fourier transforms are well defined.

Note that this operation translates each subray onto an incoming ray that propagates in the same direction, analogous to diagonal frequency domain fast multipole translation operators.

(iii) Evaluate the fields at the observers as the incoming rays travel across the observation sphere (i.e., perform the left most convolution and summations in Eq. (53)).

Note that each subray can be at most $(2R_s'/c + T_s')/\Delta t$ time steps long. Furthermore, as discussed in Subsection 2.3, the translation function associated with each ray direction is $(4R_s'/c + T_s')/\Delta t$ time steps long. By virtue of the choice $cT_s' \propto R_s'$, both the subray duration and the translation function length scale as $O(M_t')$. From Eq. (32), it is seen that the number of ray directions D_s equals $\sum_{n=0}^{M'}(2M_n + 1)$. Using Eqs. (36)–(38), it can be shown that D_s is proportional to the surface area of each sphere, i.e., $D_s \propto (R_s'/(c\Delta t))^2$.

Since the aggregation step maps M_s source subsignals onto D_s subrays, its computational cost scales as $O(M_t' M_s D_s)$. The dominant cost in the translation step is due to the convolution and scales as $O(M_t' \log M_t')$ if evaluated using an FFT. This operation is performed for all D_s directions, yielding a computational complexity of $O(D_s M_t' \log M_t')$. The disaggregation step has the same complexity as the aggregation step.

For a surface scatterer, the number of sources or observers in a sphere is proportional to the surface area of the sphere, i.e., $M_s \propto (R_s'/(c\Delta t))^2$. This implies that $M_t' \propto \sqrt{M_s}$ and that $D_s \propto M_s$. It may be verified that the cost of the aggregation and dissagregation processes dominates that of the translation process and that the cost of evaluating the observed fields for one subsignal using PWTD algorithm scales as $O(M_t' M_s^2)$. Hence, the cost of evaluating the fields due to all L subsignals scales as $O(N_t M_s^2)$. This cost is no less than that of the classical algorithm. Nonetheless, the PWTD scheme permits the reuse of SST information, which results in a reduction of the computational complexity when applied in an integral-equation setting.

However, as noted previously, not all outgoing rays contribute to the observed fields if use is made of the windowed character of the translation operator. In fact, the number of subrays that needs to be translated shrinks to a constant as the ratio of the distance between the spheres and the sphere radii increases. In these circumstances, D_s can be omitted in the above complexity estimates; hence, the computational complexity of computing the fields associated with one time interval scales as $O(M_t' M_s)$, and that of all L subsignals combined scales as $O(N_t M_s)$.

A series of numerical experiments was conducted to validate and examine accuracy versus efficiency trade-offs in the PWTD algorithm. To this end, the fields due to a set of point sources are calculated using the PWTD scheme and compared to the exact fields. In

what follows, all source functions are generated using the Gaussian pulse

$$g(t) = e^{-(t-7.75\sigma)^2/2\sigma^2}. \tag{54}$$

The variance σ is fixed at 2.12 ns, which yields a pulse with a duration (full width between half maximum) of 5 ns. For all practical purposes, this pulse can be assumed to be bandlimited to $\omega_{\max} = 600\pi \times 10^6$ rad/s. The source and observation spheres are of radius $R_s = 1$ m and are separated by $R_c = 20$ m. The time step size Δt is fixed at 0.5 ns and the wave speed is chosen to be $c = 3 \times 10^8$ m/s. For a sampled field representation, this choice of parameters yields $t_l^{\text{trans}} = 120\Delta t + lT_s - 2p_l\Delta t$.

As a first test, the fields due to two sources located at s1 and s2, as shown in the inset of Fig. 5a, are evaluated at two observer locations, o1 and o2. The time signatures of the sources are $f^j(t) = g(t) + 0.5g(t - 3 \times 10^{-8})$, $j = 1, 2$. In accordance with (21), T_s is chosen to be $6\Delta t$ which results in $\theta_{\text{int}} = 54.9^\circ$ by the equality in (22). As can be seen in Fig. 5a, the PWTD results are in excellent agreement with the exact fields. The fields due to the first pulse, $g(t)$, are observed for $t < 98$ ns, and those due to the second pulse, $0.5g(t-3\times10^{-8})$, appear later. Figure 5b shows the observed fields obtained by translating the subrays at $t = 30\Delta t + lT_s - 2p_l\Delta t < t_l^{\text{trans}}$. As expected, early translation of subrays has produced ghost signals. The ghosts due to $g(t)$ are seen for $t < 67$ ns and those due to $0.5g(t - 3 \times 10^{-8})$ corrupt the observed fields in the interval 75 ns $< t < 98$ ns.

Next, several tests were conducted to check the accuracy of the PWTD algorithm. For this purpose, six sources with time signatures $f^j(t) = g(t)$, $j = 1, \ldots, 6$, were distributed in the y-z plane on the surface of the source sphere. The radiated fields were evaluated throughout a 12 m $\times$ 12 m region in the y-z plane centered about the observation sphere center. The normalized error in each observer response was calculated by dividing the L_2 norm of the difference between the exact fields and those computed using the PWTD algorithm by the L_2 norm of the exact fields. The parameters defining the temporal and spherical interpolation functions, and an estimate of the truncation error introduced by the use of these interpolants are tabulated in Table 1 along with the average error throughout the observation sphere. It is seen that the error in the observed fields is of the same order as the error introduced by the interpolations. This implies that, as expected, the difference between the analytical and the PWTD solutions depends solely on the error due to interpolation and can be reduced to arbitrary precision. The errors for Cases B, D, F, and H of Table 1 are plotted throughout the square observation domain in Fig. 6. The location of the observation sphere is also depicted in these figures, and it is seen that for all four cases the desired accuracy is obtained throughout the observation sphere.

3.2. *Two-Level Plane Wave Time Domain Algorithm*

Now that the applicability of the PWTD algorithm has been verified for a pair of source and observation groups, we will demonstrate that this algorithm results in a reduction in computational complexity when applied to the analysis of scattering from large surfaces. The PWTD algorithm is intended to be used in conjunction with time domain integral-equation schemes like MOT. In this subsection, the computational complexity of the two-level PWTD algorithms will be derived. This analysis is akin to that used in illustrating the computational complexity of the frequency-domain FMM technique [36, 37].

In order to reduce the computational complexity of the classical MOT algorithm, the scatterer is subdivided into N_g subscatterers or groups, each of which contains approximately $M_s \propto N_s/N_g$ sources. If two subscatterers are separated by less than a preset distance, these

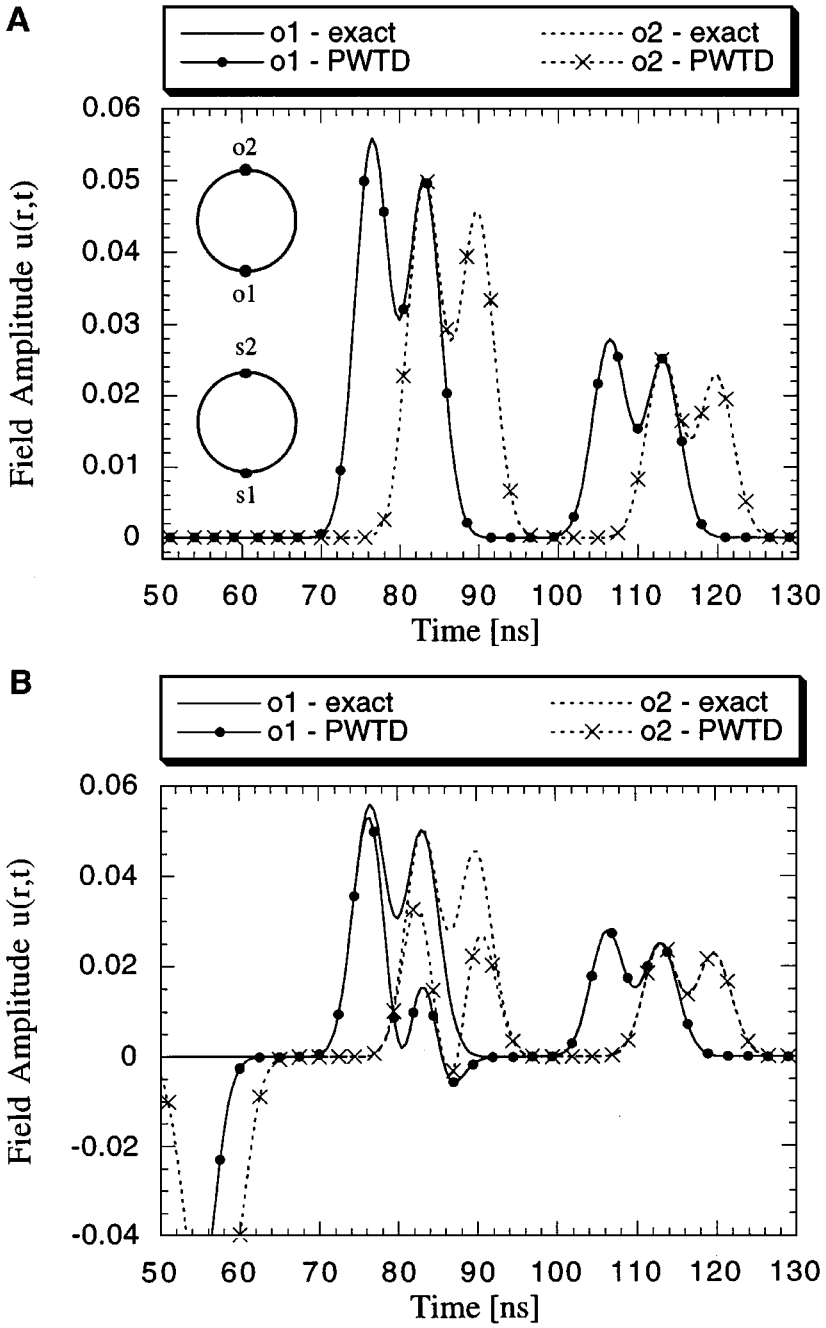

FIG. 5. Observer responses at o1 and o2 due to sources at s1 and s2 for (a) correct t_l^{trans} and (b) small t_l^{trans}.

are said to reside in each other's near-field, and their interactions are computed using the classical MOT scheme since it becomes impossible to choose a cT_s'/R_s' of $O(1)$ that satisfies constraints (21) and (22). All other subscatterer pairs are said to reside in each other's far-field. The cost associated with the computation of the near-fields, C_{NF}, is proportional to the square of the number of unknowns per group, the number of groups, and the total number

TABLE 1

Estimates of Relative Errors ε_t and ε_s Introduced by Temporal and Spatial Prolate Interpolations, Respectively, and the Average Normalized Error in Observed Fields in the Observation Sphere

Case	χ_o	p_t	χ_1	χ_2	p_s	ε_t	ε_s	Average error
A	2.17	4	1.25	2.5	4	6.16×10^{-3}	8.03×10^{-3}	1.83×10^{-3}
B	2.17	6	1.25	3.2	5	1.55×10^{-4}	1.79×10^{-4}	1.99×10^{-4}
C	2.17	8	1.25	2.9	7	5.46×10^{-5}	2.02×10^{-5}	4.20×10^{-5}
D	2.17	11	1.25	3.2	8	1.48×10^{-6}	1.43×10^{-6}	2.41×10^{-6}
E	2.17	13	1.25	3.9	8	2.37×10^{-7}	3.60×10^{-7}	2.50×10^{-7}
F	2.17	15	1.25	4.8	9	1.30×10^{-8}	1.11×10^{-8}	1.18×10^{-8}
G	2.17	17	1.25	5.1	9	1.04×10^{-9}	1.60×10^{-9}	5.15×10^{-9}
H	2.17	19	1.25	5.4	10	2.22×10^{-10}	9.31×10^{-11}	3.01×10^{-10}

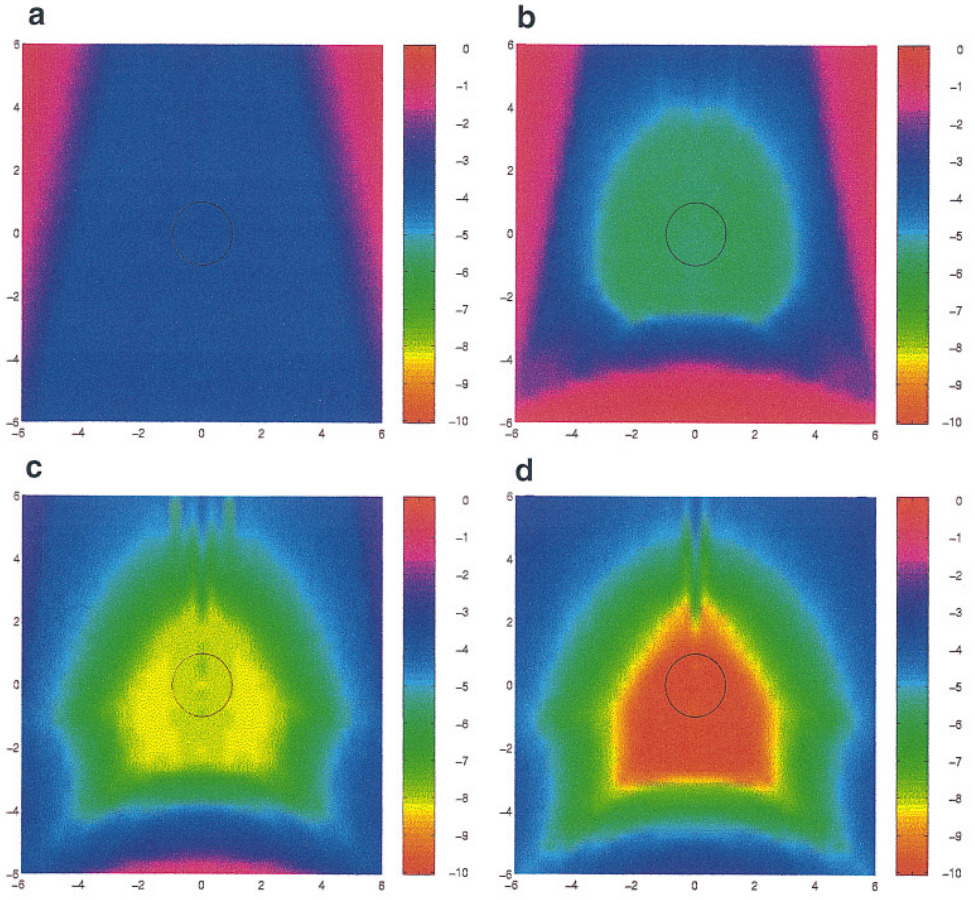

FIG. 6. Logarithm (base 10) of normalized errors observed in a 12 m × 12 m region enclosing the observation sphere (black circle) for several cases tabulated in Table 1. (a) Case B. (b) Case D. (c) Case F. (d) Case H.

of time steps in the analysis:

$$\begin{aligned} C_{NF} &\propto (\#\ \textit{of groups}) \times (\#\ \textit{of unknowns per group})^2 \times (\#\ \textit{of time steps}) \\ &\propto N_g M_s^2 N_t \\ &\propto \left(\frac{N_s}{M_s}\right) M_s^2 N_t \\ &\propto N_s M_s N_t. \end{aligned} \tag{55}$$

Interactions between remote groups are accounted for by using the three-stage procedure consisting of aggregation, translation, and disaggregation. During the aggregation stage, a separate set of outgoing subrays is constructed for each source group and for each time interval. During the translation stage, outgoing subrays are convolved with the translation functions on a direction-by-direction basis for each far-field group pair, and the resulting plane waves are added onto the incoming rays impinging on an observation group. During the disaggregation stage, the fields at the observers are reconstructed by projection of the incoming rays onto the observer points. Note that, as the disaggregation process is the reverse of the aggregation process, its cost is comparable to that of the aggregation step. Let $C_{FF}^{1,3}$ denote the total cost associated with first and third stages. Then,

$$\begin{aligned} C_{FF}^{1,3} &\propto (\#\ \textit{of groups}) \times (\#\ \textit{of unknowns per group}) \\ &\quad \times (\#\ \textit{of ray directions}) \times (\#\ \textit{of time steps}) \\ &\propto N_g M_s D_s N_t \\ &\propto \left(\frac{N_s}{M_s}\right) M_s M_s N_t \\ &\propto N_s M_s N_t, \end{aligned} \tag{56}$$

where it is assumed that $D_s \propto M_s$ as discussed above. The cost of the translation process C_{FF}^2 is

$$\begin{aligned} C_{FF}^2 &\propto (\#\ \textit{of groups})^2 \times (\#\ \textit{of ray directions}) \\ &\quad \times (\#\ \textit{of time intervals}) \times (\textit{cost per subray translations}) \\ &\propto N_g^2 D_s L M_t' \log M_t' \\ &\propto \left(\frac{N_s}{M_s}\right)^2 M_s N_t \log M_s \\ &\propto \frac{N_s^2}{M_s} N_t \log M_s, \end{aligned} \tag{57}$$

where it was assumed that the translation convolution was performed using an FFT, that $M_t' \propto \sqrt{M_s}$ as discussed earlier, and that $L \propto N_t / M_t'$. The total cost associated with the computation of the fields at all the observers is equal to

$$\begin{aligned} C_T &= C_{NF} + C_{FF} \\ &= C_{NF} + C_{FF}^{1,3} + C_{FF}^2. \end{aligned} \tag{58}$$

It can be verified that for the algorithm described above, the optimal number of unknowns per group is $M_s \propto N_s^{1/2}$, and the total computation time scales as

$$C_T \propto N_t N_s^{3/2} \log N_s. \tag{59}$$

The cost of this algorithm can be further reduced if one makes use of the fact that not all plane waves need to be translated from one group to another. Indeed, as the interacting groups move further apart, the number of plane wave components which participate shrinks to a constant.[1] This yields

$$C_{FF}^2 \propto N_t \frac{N_s^2}{M_s^2} \log M_s. \tag{60}$$

Using this expression in Eq. (58), the optimal value of M_s is found to be $N_s^{1/3}$, and the total cost of the field computation scales as

$$C_T \propto N_t N_s^{4/3} \log N_s. \tag{61}$$

Note that the computational costs of both the nonwindowed and the windowed two-level PWTD scale more favorably than those of the classical MOT and FDTD algorithms.

3.3. *Multilevel Plane Wave Time Domain Algorithm*

It is well known that the computational complexity of two-level frequency-domain FMM algorithms can be further reduced through a divide-and-conquer strategy by casting the algorithm in a multilevel framework. This is also true for fast plane wave time domain algorithms.

To compute the fields using a multilevel strategy, the surface is embedded in a box, which is subdivided into eight child boxes or groups. Each of the nonempty child boxes is again subdivided into eight boxes, and this process is continued recursively until the finest level is reached. At the finest level, each box contains a fixed number of sources which are independent of the problem size. The number of levels N_l is proportional to $\log N_s$. For levels $i = 1, \ldots, N_l$, let $N_g(i)$ denote the number of nonempty groups, $M_s(i)$ the average number of sources in each group, $D_s(i)$ the number of ray directions associated with a group, and $R_s(i)$ the group dimension. Also, the duration of the subray at level i, $M_t'(i)$, is assumed to be proportional to $\sqrt{M_s(i)}$. Finally, let $L(i) \propto N_t/M_t'(i)$ denote the number of time intervals associated with level i. Assuming that levels are numbered starting from the finest level upward, for a surface scatterer, $N_g(i+1) \propto N_g(i)/4$ and $M_s(i+1) \propto 4M_s(i)$. We also assume that $N_g(1) \propto N_s$, and that $M_s(1)$ and $R_s(1)$ are of $O(1)$. As i increases, $L(i)$ shrinks; hence fewer time intervals are associated with higher levels. Subrays at each level can be constructed by concatenating (partially overlapping) subrays that have been constructed at lower levels. As before, it can be shown that $M_s(i) \propto D_s(i) \propto (R_s(i)/(c\Delta t))^2$. At any level, two boxes are said to reside in each other's near-field if they are separated by no more than a preset, fixed number of boxes. All other box pairs are said to reside in each other's far-field.

[1] Note that, for source and observation spheres that are not separated by a distance that is very large compared to the sphere radius, the number of rays that need to be translated becomes larger than the constant assumed in the derivation of (60). However, it can be shown through a more rigorous derivation that this effect does not alter the above derived complexity estimate for C_{FF}^2.

The total cost of the field computation is again a sum of a near-field cost C_{NF} and a far-field cost C_{FF}. At the finest level, fields are computed directly for all sources and for all observers that reside in each other's near-field for all time steps. The cost of this operation is

$$\begin{aligned} C_{NF} &\propto (\#\ \textit{of finest level groups}) \times (\#\ \textit{of sources per finest level group})^2 \\ &\quad \times (\#\ \textit{of time steps}) \\ &\propto N_g(1) M_s^2(1) N_t \\ &\propto N_s N_t. \end{aligned} \tag{62}$$

The cost of computing the far-field interactions is again composed of aggregation, translation, and dissagregation costs. However, in contrast to the two-level algorithm outlined above, these costs are now distributed over all N_l levels.

First, consider the cost of computing the outgoing rays. At any given level, the outgoing rays associated with a group are constructed by (i) interpolating the spectra of its children to the ray density prescribed by the dimension of their parent group, (ii) concatenating consecutive child subrays two-by-two, and (iii) shifting all ray origins from child box centers to parent box centers. Similar operations are required when constructing incoming rays. The total cost of constructing the outgoing and incoming rays is

$$\begin{aligned} C_{FF}^{1,3} &\propto \sum_{i=1}^{N_l} \left\{ \begin{array}{l} (\#\ \textit{of groups at level } i) \times (\#\ \textit{of directions at level } i) \\ \quad \times (\textit{subray length at level } i) \times (\#\ \textit{of time intervals at level } i) \end{array} \right\} \\ &\propto \sum_{i=1}^{N_l} N_g(i) D_s(i) M_t'(i) L(i) \\ &\propto \sum_{i=1}^{N_l} \left(\frac{N_s}{M_s(i)} \right) M_s(i) N_t \\ &\propto N_t N_s \log N_s. \end{aligned} \tag{63}$$

To compute fields at observers, outgoing rays are translated between all group pairs that reside in each other's far-field and whose parents reside in each other's near-field. The cost of translating subrays is proportional to

$$\begin{aligned} C_{FF}^{2} &\propto \sum_{i=1}^{N_l} \left\{ \begin{array}{l} (\#\ \textit{of groups at level } i) \times (\#\ \textit{of ray directions at level } i) \\ \quad \times (\#\ \textit{of time intervals at level } i) \\ \quad \times (\textit{cost per subray translation at level } i) \end{array} \right\} \\ &\propto \sum_{i=1}^{N_l} N_g(i) D_s(i) L(i) M_t'(i) \log M_t'(i) \\ &\propto N_t N_s \sum_{i=1}^{N_l} \log M_s(i) \\ &\propto N_t N_s M_s(1) (\log 2^0 + \log 2^1 + \log 2^2 + \cdots + \log 2^{\log N_s}) \\ &\propto N_t N_s (1 + 2 + \cdots + \log N_s) \\ &\propto N_t N_s \log^2 N_s. \end{aligned} \tag{64}$$

Comparing the expressions for C_{NF}, $C_{FF}^{1,3}$, and C_{FF}^{2}, it is seen that the total cost of the multilevel PWTD algorithm is dominated by C_{FF}^{2}; hence,

$$C_T \propto N_t N_s \log^2 N_s. \tag{65}$$

This cost can be further reduced if use is made of the truncated version of $\Psi_n(\theta)$ to form the translation functions (see Subsection 2.3). For sufficiently large scatterers, the length of these truncated translation functions scales as $(R_c/c)p_s\Delta\theta\theta_{\text{int}}$. Since, in a multilevel setting, R_c scales as R_s, $\Delta\theta$ scales as $1/R_s$, and p_s and θ_{int} remain constant for all levels, the translation function length is of $O(1)$. Therefore, directly convolving each subray with the translation function will be more efficient than using an FFT, reducing the cost per subray translation in C_{FF}^{2} from $O(M_t'(i)\log M_t'(i))$ to $O(M_t'(i))$. This results in a total complexity of

$$C_T \propto N_t N_s \log N_s. \tag{66}$$

4. SUMMARY

This paper presented PWTD procedures that permit the fast computation of transient fields radiated by surface bound sources. These schemes rely on time domain diagonalized translation operators and can be considered an extension of the frequency domain fast multipole method to the time domain. The practical implementation of the PWTD algorithm has been elucidated, and examples illustrating its accuracy have been presented. It has been shown that the error in the observer fields depends solely on the approximations introduced by the interpolation functions, whose parameters can be chosen in accordance with any desired error criterion. The PWTD algorithms complement integral-equation-based source updating schemes and reduce the computational complexity associated with the analysis of surface scattering phenomena from $O(N_t N_s^2)$ to $O(N_t N_s^{4/3}\log N_s)$ for two-level and to $O(N_t N_s \log N_s)$ for multilevel schemes.

Two-level and multilevel PWTD algorithms have been applied to the analysis of large-scale acoustic and electromagnetic scattering problems, and our results will be reported elsewhere. Work toward extending this algorithm to multilayered media and the hybridization of the PWTD algorithm with shooting and bouncing ray methods is in progress.

ACKNOWLEDGMENTS

The authors thank Professor W. C. Chew for his comments to the current manuscript. This research was supported by the Air Force Office for Scientific Research via the MURI program under Contract F49620-96-1-0025; the NSF under Grant ECS 95-02138; and the Gebze Institute of Technology, Turkey.

REFERENCES

1. L. B. Felsen, Ed., *Transient Electromagnetic Fields* (Springer-Verlag, Berlin, 1976).
2. M. Tygel and P. Hubral, *Transient Waves in Layered Media* (Elsevier, Amsterdam, 1987).
3. B. P. Rynne, Time domain scattering from arbitrary surfaces using the electric field integral equation, *J. Electromagn. Waves Appl.* **5**, 93 (1991).
4. S. M. Rao and D. A. Wilton, Transient scattering by conducting surfaces of arbitrary shape, *IEEE Trans. Antennas Propag.* **39**, 56 (1991).

5. E. K. Miller, A selective survey of computational electromagnetics, *IEEE Trans. Antennas Propag.* **36**, 1281 (1988).
6. E. Heyman, Time-dependent plane-wave spectrum representations for radiation from volume source distributions, *J. Math. Phys.* **37**, 658 (1996).
7. Y. Dai, E. J. Rothwell, K. M. Chen, and D. P. Nyquist, Time-domain imaging of radar targets using algorithms for reconstruction from projections, *IEEE Trans. Antennas Propag.* **45**, 1227 (1997).
8. A. Shlivinski, E. Heyman, and R. Kastner, Antenna characterization in the time domain, *IEEE Trans. Antennas Propag.* **45**, 1140 (1997).
9. K. S. Kunz and R. J. Luebbers, *The Finite Difference Time Domain Method for Electromagnetics* (CRC Press, Boca Raton, 1993).
10. J.-F. Lee, R. Lee, and A. Cangellaris, Time-domain finite-element methods, *IEEE Trans. Antennas Propag.* **45**, 430 (1997).
11. M. J. Lesha and F. J. Paoloni, Transient scattering from arbitrary conducting surfaces by iterative solution of the electric field integral equation, *J. Electromagn. Waves Appl.* **10**, 1139 (1996).
12. M. J. Bluck and S. P. Walker, Time-domain BIE analysis of large three-dimensional electromagnetic scattering problems, *IEEE Trans. Antennas Propag.* **45**, 894 (1997).
13. G. Manara, A. Monorchio, and R. Reggiannini, A space-time discretization criterion for a stable time-marching solution of the electric field integral equation, *IEEE Trans. Antennas Propag.* **45**, 527 (1997).
14. P. J. Davies, Numerical stability and convergence of approximations of retarded potential integral equations, *SIAM J. Num. Anal.* **31**, 856 (1994).
15. W. Pinello, A. Ruehli, and A. Cangellaris, Stabilization of time domain solutions of EFIE based on partial element equivalent circuit models, in *Proc. IEEE Antennas Prop. Society In. Symp., Montreal* (1997), p. 966.
16. R. Coifman, V. Rokhlin, and S. Wandzura, The fast multipole method for the wave equation: A pedestrain approach, *IEEE Antennas Propag. Mag.* **35**, 7 (1993).
17. V. Rokhlin, Diagonal forms of translation operators for Helmholtz equation, *Appl. Comput. Harmon. Anal.* **1**, 82 (1993).
18. J. M. Song and W. C. Chew, Multilevel fast-multipole algorithm for solving combined field integral equations of electromagnetic scattering, *Microwave Opt. Technol. Lett.* **10**, 14 (1995).
19. V. Rokhlin, Sparse diagonal forms for translation operators for the Helmholtz equation in two dimensions, Technical Report YALEU/DCS/RR-1095, Department of Computer Science, Yale University (1995).
20. F. X. Canning, The impedance matrix localization (IML) method for moment-method calculations, *IEEE Antennas Propag. Mag.* **32**, 18 (1990).
21. E. Michielssen and A. Boag, A multilevel matrix decomposition algorithm for analyzing scattering from large structures, *IEEE Trans. Antennas Propag.* **44**, 1086 (1996).
22. T. B. Hansen, Spherical expansions of time-domain acoustic fields: Application to near-field scanning, *J. Acoust. Soc. Am.* **98**, 1204 (1995).
23. E. Heyman, Time-dependent multipoles and their application for radiation from volume source distributions, *J. Math. Phys.* **37**, 682 (1996).
24. O. M. Buyukdura and S. S. Koc, Two alternative expressions for the spherical wave expansion of the time domain scalar free-space Green's function and an application: Scattering by a soft sphere, *J. Acoust. Soc. Am.* **101**, 87 (1997).
25. A. A. Ergin, Two compression algorithms for the marching-on-in-time solution of scattering from two-dimensional conducting strips, M.S. dissertation, Department of Electrical and Computer Engineering, University of Illinois at Urbana-Champaign (1995).
26. W. C. Chew, *Waves and Fields in Inhomogeneous Media* (Van-Nostrand/Reinhold, New York, 1990).
27. C.-C. Lu and W. C. Chew, A multilevel algorithm for solving a boundary integral equation of wave scattering, *Microwave Opt. Technol. Lett.* **7**, 466 (1994).
28. C. H. Chapman, Generalized Radon transforms and slant stacks, *Geophys. J. R. Astron. Soc.* **66**, 445 (1981).
29. S. S. Huestis, Interpolation formulas for oversampled band-limited functions, *SIAM Rev.* **34**, 477 (1992).

30. J. J. Knab, Interpolation of band-limited functions using the approximate prolate series, *IEEE Trans. Inform. Theory* **25**, 717 (1979).
31. O. M. Bucci, C. Gennarelli, and C. Savarese, Optimal interpolation of radiated fields over a sphere, *IEEE Trans. Antennas Propag.* **39**, 1633 (1991).
32. W. H. Press, S. A. Teukolsky, W. T. Vellerling, and B. P. Flannery, *Numerical Recipes in Fortran 77: The Art of Scientific Computing* (Cambridge Univ. Press, New York, 1996).
33. B. Shanker, A. A. Ergin, and E. Michielssen, Two-level plane wave time domain algorithm for fast analysis of transient scattering, Technical Report, Center for Computational Electromagnetics, University of Illinois at Urbana-Champaign (in preparation).
34. R. L. Wagner and W. C. Chew, A ray-propagation fast multipole algorithm, *Microwave Opt. Technol. Lett.* **7**, 435 (1994).
35. R. Coifman, V. Rokhlin, and S. Wandzura, Faster single-stage multipole method for the wave equation, in *10th Annual Review of Progress in Applied Computational Electromagnetics, Monterey, CA* (1994), p. 19.
36. L. Greengard and V. Rokhlin, A new version of the fast multipole method for the Laplace equation in three dimensions, *Acta Numerica*, 229 (1997).
37. V. Jandhyala, E. Michielssen, B. Shanker, and W. C. Chew, A combined steepest descent-fast multipole algorithm for the analysis of three-dimensional scattering by rough surfaces, *IEEE Trans. Geosci. Remote Sensing* **36**, 738 (1998).